UDC: 539.232
Review article

THE EFFECT OF PRECURSOR SYNTHESIS TEMPERATURE ON SOL-GEL CZTS SPIN-COATED THIN FILMS PROPERTIES

Ramadan ALITI[1,4*], Yoganash PUTTHISIGAMANY[2], Mohd SUKOR SU'AIT[2], Azizan Bin AHMAD[3], Kazi Sajedur RAHMAN[2], Puvaneswaran CHELVANATHAN[2], Mimoza RISTOVA[1]

[1] *Institute of Physics, Faculty of Natural Sciences and Mathematics, Ss. Cyril and Methodius University*
[2] *Solar Energy Research Institute (SERI), The National University of Malaysia*
[3]*Department of Chemical Sciences, Faculty of Science and Technology, Universiti Kebangsaan Malaysia*
[4] *Department of Physics, Faculty of Natural Sciences and Mathematics, University of Tetovo*
[*]*Corresponding Author: e-mail: ramadan.aliti@unite.edu.mk*

Abstract

The non-vacuum sol-gel method for synthesizing CZTS thin films has proven to be a simple, cost-effective, and highly efficient approach that can be utilized across a wide range of temperatures. In this study, our focus was on synthesizing CZTS at room temperature (RT) and 1500C, with the chemical reagents sequentially mixed at 30-minute intervals. The spin coating process was employed to deposit the solutions onto Na-free substrate glasses to obtain thin films. X-ray diffraction (XRD) patterns demonstrate the formation of CZTS crystallinity, exhibiting variations in crystallite size and grain morphology, which were further confirmed by SEM images. Comparing the CZTS thin films synthesized at RT and 1500C, it was observed that the RT samples exhibited larger grain size, smaller crystal size, improved crystallinity, and a greater amount of surface cracking. Raman spectroscopy analysis confirmed the presence of CZTS Raman spectra, with well-defined main peaks observed at 335.3 cm-1 and 327.6 cm-1 for RT and 1500C, respectively. These findings underscore the significance of precursor synthesis temperature in sol-gel CZTS spin-coated thin films, and suggest that further in-depth analysis of this parameter is warranted for future investigations.

Keywords: CZTS, sol-gel, thin films, phase

1. Introduction

CZTS (Copper-Zinc-Tin-Sulfur) or Cu2ZnSnS4 is an important material due to its abundance in the Earth's crust, non-toxicity, and low cost. It is a p-type semiconductor with a direct band gap in the optimal range of 1.0 eV to 1.5 eV and exhibits a high absorption coefficient ($> 10^4\ cm^{-1}$), making it an excellent candidate for the absorber layer in solar cells (Chen et al. 2009; Guo et al. 2014). A notable advantage of CZTS is the wide range of synthesizing methods available, including both vacuum and non-vacuum techniques (Lai et al. 2017). Various methods such as magnetron and hybrid sputtering, evaporation, spray pyrolysis, chemical vapor deposition, co-evaporation, and spin-coated deposition have been utilized for growing CZTS absorber layers (Dwivedi et al. 2021; Enayati Maklavani e Mohammadnejad 2020).

Among these methods, the non-vacuum sol-gel approach has gained attention for its simplicity, cost-effectiveness, and effectiveness over a range of temperatures. CZTS thin films synthesized using the sol-gel method have emerged as a promising, environmentally friendly, and low-cost alternative to conventional solar cell materials (Tanaka et al. 2007; Todorov et al. 2020). The sol-gel method can be easily combined with spin coating, offering advantages such as simplicity, low cost, uniformity of thin films, precise control over film thickness, versatility in precursor solutions, and compatibility with large-area deposition. Although the maximum theoretical efficiency of CZTS-based solar cells is 30.3%, experimental achievements have reached

a maximum efficiency of 13.6% due to several challenges (Gong et al. 2021). Key challenges include stoichiometry control (addressing defects, structural variations, and the presence of secondary phases), surface defects, interface quality, and sulfur vacancies (He et al. 2021; Romanyuk et al. 2019; Chen et al. 2013). Overcoming these challenges requires further research and optimization of sol-gel process parameters, precursor chemistry, sulfurization methods, and post-deposition treatments. Advanced characterization techniques and device engineering strategies are also essential to fully exploit the potential of CZTS thin films for solar energy conversion (Enayati Maklavani e Mohammadnejad 2020; He et al. 2021; Kumar 2021).

This study focuses on investigating the influence of CZTS precursor synthesis temperature on the morphological and structural properties of thin films. By employing the sol-gel method and optimized annealing treatment, we analyzed the effects of varying precursor concentrations, reaction times, temperatures, and other parameters on the stoichiometry of the resulting CZTS thin films.

2. Experimental details

2.1. CZTS thin films fabrication: The CZTS precursor solution was prepared using the sol-gel method at room temperature (RT) (sample marked as RT) and on a hot plate at 150°C (sample marked as150°C). To prepare sol-gel solution, 1.1 M of copper acetate dihydrate ($Cu(CH_3COO)_2 \cdot H_2O$, 98%), 0.7 M of zinc acetate dihydrate ($Zn(CH_3COO)_2 \cdot 2H_2O$, 98%), 0.6 M of tin chloride ($SnCl_2 \cdot H_2O$, 95%), and 2.4 M thiourea (CH_4N_2S, 95%) were sequentially dissolved in 10 ml of 2-methoxyethanol, with 30 minutes between adding each following precursor from the sequence above. After about 48 hours, monoethanolamine (MEA) was added in a 1:1 ratio to the zinc acetate dihydrate to achieve the desired density for the spin coating process. Na-free glass substrates were prepared by rubbing them with deionized water and cleaning them in an 80°C ultrasonic bath using ethanol, acetone, and again ethanol for 10 minutes each, followed by 20 minutes in deionized water. The substrates were then dried with a spun gun of N_2 and heated on a 120°C hot plate before being placed in an ozone cleaner for 10 minutes. The spin-coated thin films were preheated in an open-air environment at 210°C for 2 minutes per layer with a substrate rotation speed of 2500 rpm. For the annealing process, the samples were placed on a small graphene box containing approximately 100 mg of sulphur (S) and 20 mg of tin sulphide (SnS_2). The graphene box with the samples, under a N_2 atmosphere, was placed in a tubular furnace (OTF-1200X, MTI-USA) and annealed at 580°C for 30 minutes. The base pressure, working pressure, and ramp-rate were maintained at 115 mTorr, 400 Torr, and 10°C/min, respectively. The two different samples, subject to this study differ only in the hot plate spin coating temperature, RT or 150^0C.

2.2. Characterizations methods. The morphology and chemical composition of the CZTS thin films synthesized at room temperature, RT and 150°C samples were characterized using a Carl Zeiss Merlin field emission scanning electron microscope (FESEM-EDX) operated at 3 kV. This microscope allowed for high-resolution imaging and elemental analysis of the samples. Raman spectra of the thin films were obtained using a Thermo Scientific DXR2xi Raman Imaging Microscope. This technique provided information about the molecular vibrations and crystal structure of the CZTS material. To analyse the crystalline properties of the thin films, X-ray diffraction (XRD) measurements were performed using a Bruker AXS-D8 Advance system equipped with a Cu-Kα source ($\lambda = 1.5406$ Å). The measurements covered 2 Theta angles ranging from 15° to 80°, allowing for the determination of the crystal structure and phase composition of the CZTS thin films. Grain size was established using an SEM image length measuring two dimensions (one longest and one shortest) using software ImageJ, available as an open resource on the internet.

3. Results and discussion

3.1. Chemical composition analysis of thin films: The chemical composition of the thin films synthesized at room temperature, RT sample and 150°C sample was determined using energy-dispersive X-ray spectroscopy (EDX), and the atomic percentages (at%) are presented in Table 1 and illustrated in Figure 1. From Table 1, it is evident that the composition of the films obtained at RT and 150°C is nearly identical. Slight differences can be observed in the atomic percentages of zinc (Zn) where the RT sample shows slightly higher contents. Also, the Cu content is dominant for the RT sample. This observation was expected since strict ratio considerations of Cu-poor composition with (Cu/Sn)<2 and (Cu/(Zn+Sn))<0.9, and a Zn-rich composition with (Zn/Sn)>1 have been proposed by earlier researchers to achieve the stable phase of CZTS thin films [11, 13]. As can be seen in Table 1 and Figure 1, the obtained values deviate from the proposed criteria, with the copper (Cu) content (2.28 for RT and 2.13 for the 150^{0}C) slightly exceeding the recommended Cu/Sn<2 and Cu/(Zn+Sn)<0.9 ratios, which can be attributed to the loss through evaporation of Sn during the annealing process. Nevertheless, the closer Cu/Sn ratio to the recommended is found for 150^{0}C Sample.

Table 1. Elemental atomic composition (in at%) and their ratio of Sample RT and Sample 150^{0}C CZTS thin films measured by FESEM-EDX

Sample	S, at%	Cu, at%	Zn, at%	Sn, at%	Cu/Sn	Cu/(Zn+Sn)	Zn/Sn
Sample RT	46.5	27	14.7	11.8	2.28	1.02	1.25
Sample 150^{0}C	47.7	25.8	14.4	12.1	2.13	0.97	1.19

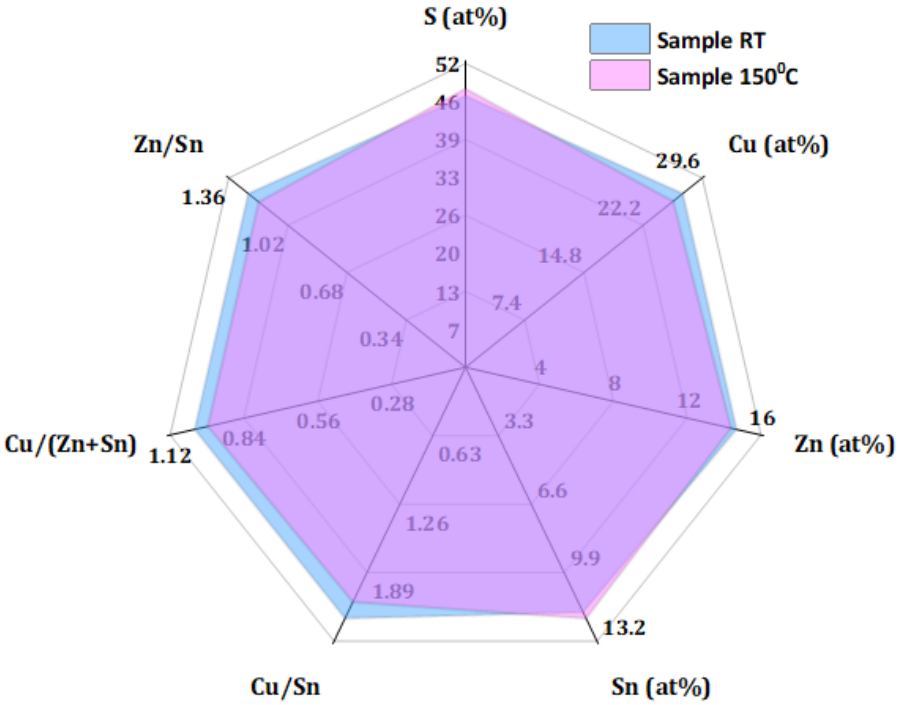

Figure 1. Comparison of chemical composition (in at%) and some relevant ratios of Sample RT and Sample 150^{0}C CZTS thin films measured by FESEM-EDX

3.2. Thin films morphology. Figure 2 shows the SEM images of the CZTS films deposited via the spin coating process using precursors synthesized at room temperature, (a) Sample RT and (b) Sample 150°C. In both cases, pronounced cracks are observed at low magnifications, which are attributed to various factors related to solvent and substrate properties. However, despite the presence of cracks, both samples exhibit homogeneous surfaces. The notable difference between the two samples lies in the grain size. In the CZTS film synthesized at room temperature (Sample RT), grains of different sizes can be observed, with an average value of 594 nm. On the other hand, in the CZTS film synthesized at 150°C (Sample 150^0C), relatively small and uniformly sized grains are present, with an average gain size value of 218 nm. These average grain sizes are obtained from the normal grain size distribution histograms (Figure 3) based on measurements of 50 grains from the SEM images. Herein, one may conclude that the synthesis at 150^0C produces about 3 times smaller grains in diameter.

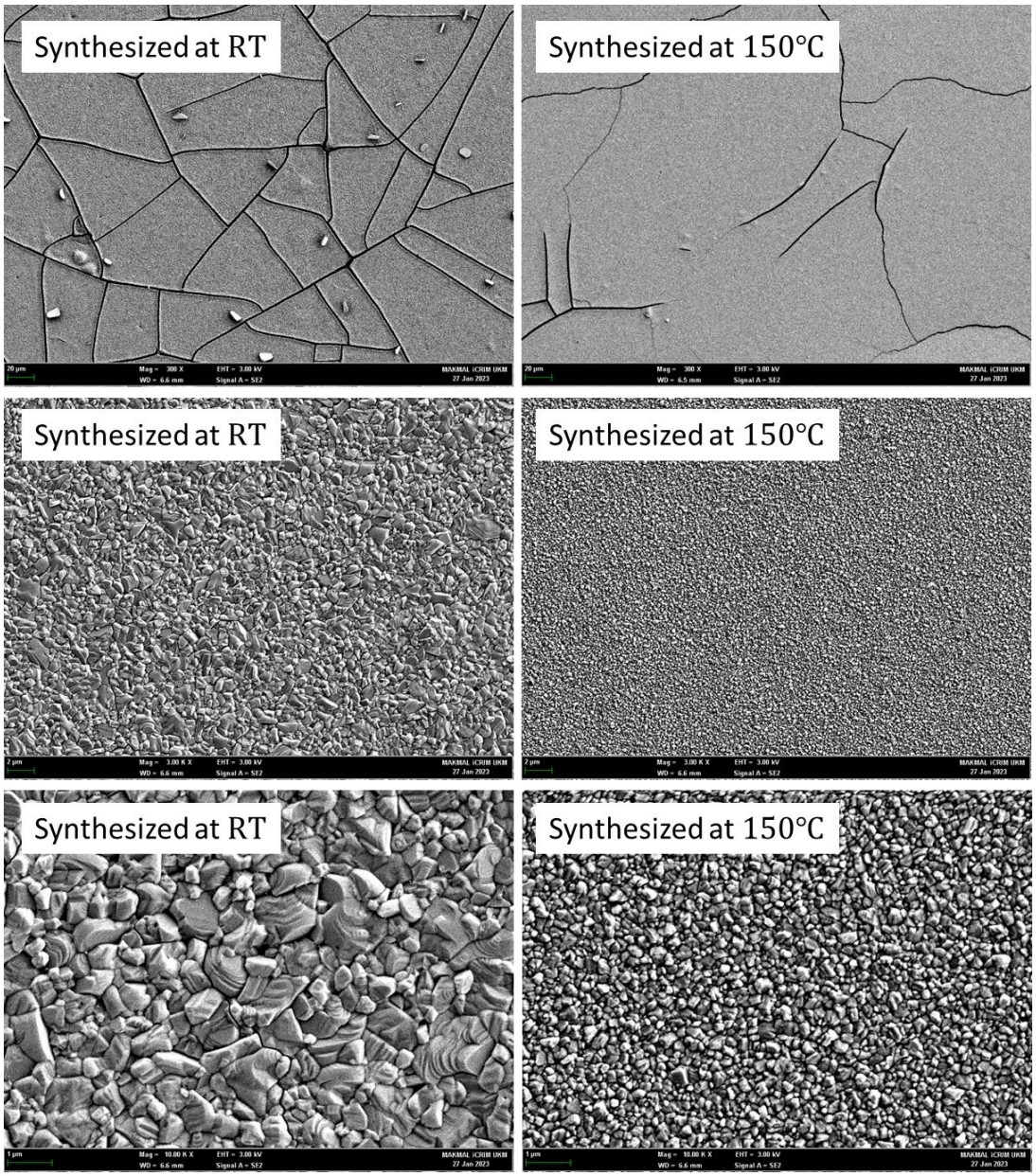

Figure 2. FESEM images of thin films prepared from precursor synthesized at **a)** room temperature (RT) and **b)** at 150°C.

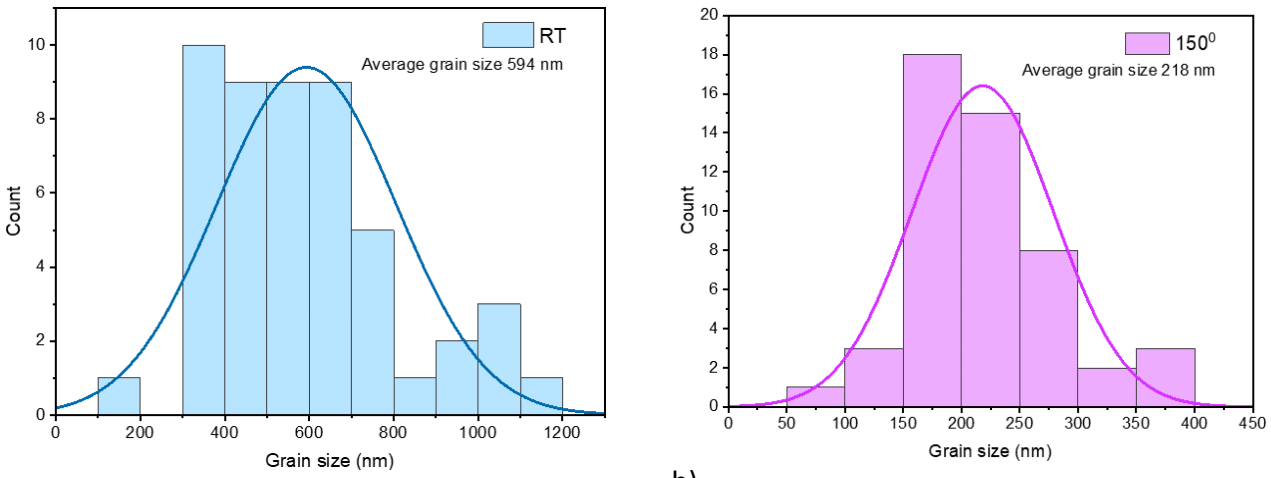

Figure 3. Grain size histograms of thin films prepared from precursor synthesized at **a)** room temperature (RT) and **b)** at 150℃.

3.3. Thin films structural characterization. Figure 4a) shows the XRD patterns of CZTS thin films fabricated using the sol-gel method. The XRD pattern of the CZTS film synthesized at room temperature (Sample RT) and the film synthesized at 150°C (Sample 150^0C). The peaks observed in the XRD pattern of the 150°C sample at diffraction angles 2θ of 18.36° (101), 28.51° (112), 29.71° (103), 33.10° (200), 47.40° (220), 56.15° (312), and 56.32° (116) correspond to the kesterite crystal phase of CZTS (JCPDS 26-0575) (Kattan et al. 2015; Ahmed et al. 2012). In the XRD pattern of the Sample RT, higher intensity peaks at the aforementioned angles and planes are observed. Herein one additional peak at 2θ=31.95° appears. This additional peak can be attributed to the presence of the secondary phase CuS_x (JCPDS 6-0464) (Chen et al. 2013; Kodigala 2014; Tiong et al. 2014; Alamri 2023). The presence of this secondary phase indicates that the RT sample has a higher degree of crystallinity. This suggests that the thin film grown from the precursor synthesized at room temperature has a more well-defined and ordered crystal structure compared to the film grown from the precursor synthesized at 150°C.

In Figure 4b), the XRD pattern of the room temperature sample (Sample RT) shows a shift of the diffraction peak (112) to lower diffraction angles, along with a slight increase in the full width at half-maximum (FWHM) value, β. This peak broadening observed in the XRD pattern indicates that the crystalline domains in the RT material are smaller in size compared to that of the 150^0C sample, and therefore a crystallite size calculations are made.

The lattice parameters of CZTS thin films were calculated combining Bragg Law $\lambda = 2d \sin\theta$, Debye Scherrer's (DS), Equation (1) and taking in consideration Millers indices (hkl) for tetragonal body-centered kesterite structure, Equation (2).

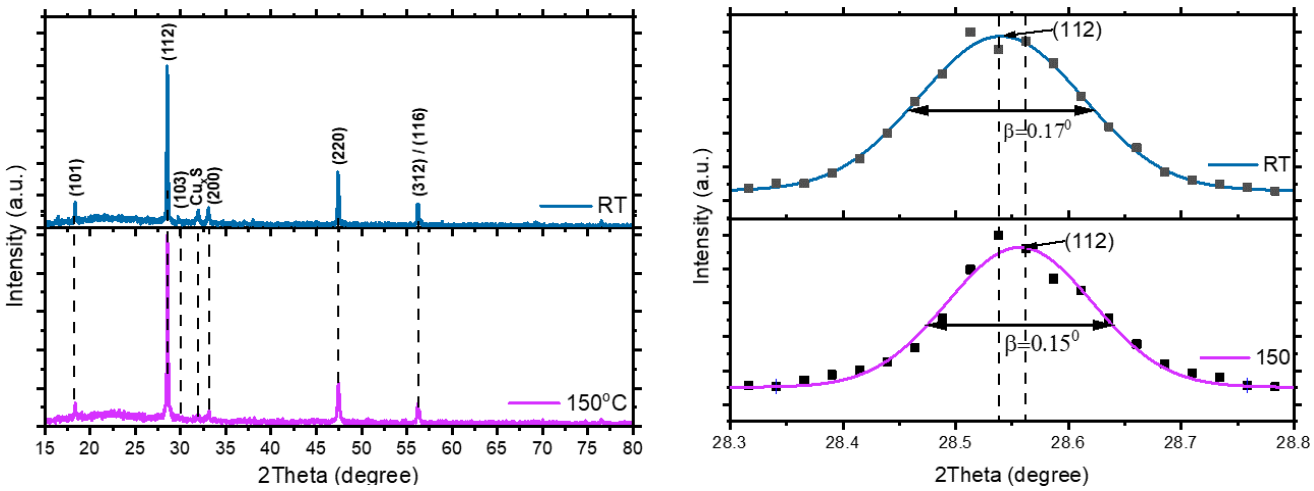

a) b)

Figure 4. a) XRD spectra and **b)** enlarged main peaks, (112) of CZTS thin films synthesized at room temperature (RT) and at 150℃

$$D = \frac{0.94\lambda}{\beta cos\theta} \quad (1)$$

$$\frac{1}{d^2} = \frac{h^2+k^2}{a^2} + \frac{l^2}{c^2} \quad (2)$$

where D is the crystallite size, β indicate the full width at half-maximum (FWHM) of the X-ray diffraction peak in radians, λ is the wavelength of the X-ray, d the interplanar spacing and θ is the Bragg's diffraction angle. The microstrain (ε) values of CZTS thin films synthesised at room temperature (Sample RT) and at 150^0C (Sample 150^0C), were obtained using Equation (3).

$$\varepsilon = \frac{\beta \cot\theta}{4} \quad (3)$$

Table 2. Lattice parameters 'a', 'c','d_{112}' and 'd_{220}' and their comparison with standard values of CZTS kesterite type, and Volume 'V', Micro-strain '$\boldsymbol{\varepsilon}$', Crystallite size 'D'.

Sample	$\boldsymbol{a}$ (Å)	$\boldsymbol{c}$ (Å)	$\boldsymbol{d_{112}}$(Å)	$\boldsymbol{d_{220}}$(Å)	$\boldsymbol{V}$ (Å^3)	$\boldsymbol{\varepsilon}$ ($\times$ $\boldsymbol{10^{-3}}$)	**D (nm)**
Sample RT	5.418	10.807	3.125	1.916	317.26	0.721	61.71
Sample 150^0C	5.417	10.794	3.123	1.915	316.72	0.641	73.96
CZTS (kesterite type) (Ito 2015; Ahmad et al. 2022)	5.427	10.871	3.135	1.919	-	-	-

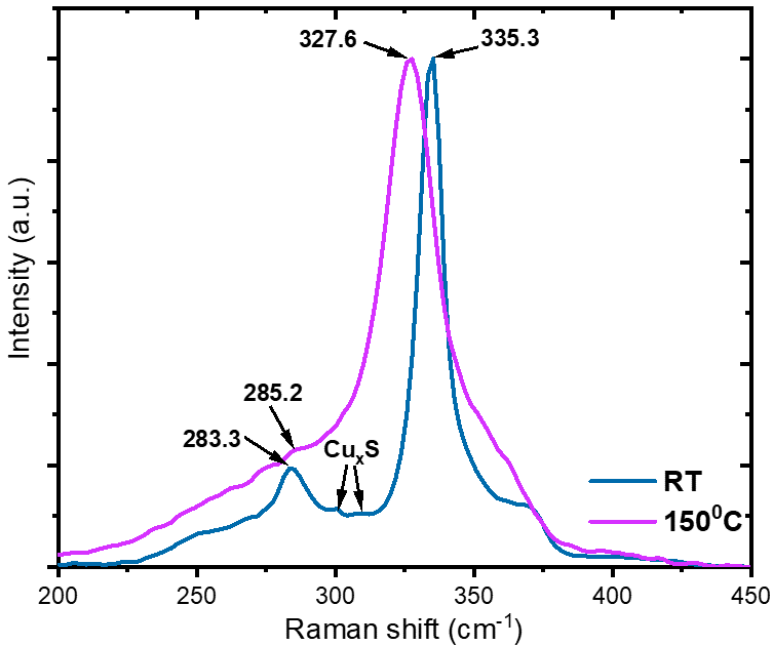

Figure 5. Raman spectra of CZTS thin films prepared from precursor synthesized at room temperature (RT) and at 150°C

Based on the data presented in Table 2, it can be concluded that the crystal lattice of Sample RT undergoes some strain, resulting in an expansion of the crystal structure along certain directions. This expansion leads to a larger *d*-spacing, causing the crystals to align preferentially in a particular direction (112) and resulting in less intense angle peaks in the XRD pattern (Ahmad et al. 2022). The analysis of the crystallite size values from the main peak (112) for both samples shows that Sample 150^{0}C has larger crystallites and a narrower main peak compared to Sample RT. As expected, the calculated crystallite size value D is greater for the sample synthesized at 150^0 (56.44 nm) compared to that synthesized at RT (50.17 nm). It has been established previously that the XRD patterns alone cannot distinguish the crystalline structure of CZTS from the secondary phases that may appear, such as Cu_2SnS_3, Cu_xS, ZnS, and SnS phases (Chen et al. 2013; Ahmoum et al. 2020; Fernandes et al. 2011). Therefore, it was necessary to apply Raman characterization. Figure 5 shows the CZTS Raman spectra, with well-defined main peaks at 335.3 cm^{-1} for Sample RT and 327.6 cm^{-1} for Sample 150^{0}C (Guo et al. 2014; Alamri 2023). A couple of prominent secondary peaks are observed at 283.3 cm^{-1} and 285.2 cm^{-1} for Sample RT and Sample 150^{0}C, respectively. These slight differences in the Raman peak positions, compared to the standard values for CZTS (338 cm^{-1} and 287 cm^{-1}), can be attributed to the stress in the thin film itself (Guo et al. 2014). The small vibrations observed in the vicinity of 300 cm^{-1} of the Raman spectrum of Sample RT are indicative of the presence and activity of the secondary phase Cu_xS, which is also identified by the XRD pattern in Figure 4(a) at $2\theta=31.95°$ (Guo et al. 2014). The absence of additional vibrations in both cases indicated the stability and strengthening of the chemical bonds within such synthesized CZTS crystalline structure.

4. Conclusions

In this study, the sol-gel method for the synthesis of CZTS thin films at room temperature (Sample RT) and at 150^{0}C (Sample 150^{0}C) was employed. The study of morphology with SEM showed that the sol-gel synthesis at 150^{0}C produces about 3 times smaller grains in diameter (compared to 594). The EDX examination proved that the 150^{0}C synthesis yields Cu/Sn closer to the recommended value (<2). i.e., 2,13 rather than 2.28 found for the RT sample. All the peaks found in the XRD patterns correspond to the kesterite crystal phase of CZTS, with the dominant crystallite orientation being along the (112) plane. Sample RT reveals one additional

diffraction peak at 2θ=31.95° appears that could be attributed to the presence of the secondary phase CuS_x indicating that the RT sample has a higher degree of crystallinity. The analysis of the crystallite size values from the main peak (112) for both samples shows that Sample 150^0C has larger crystallites and a narrower main peak compared to those of Sample RT. CZTS Raman spectra showed well-defined main peaks at 335.3 cm^{-1} for Sample RT and 327.6 cm^{-1} for Sample 150^0C.
The slight shift in the Raman peaks (main and secondary) compared to the standard values for CZTS (338 cm^{-1} and 287 cm^{-1}) could be attributed to stress within both the examined thin film structures. Typical CuS_x secondary phase peak was found only in the RT Sample, with both, XRD and Raman analysis.
As an overarching conclusion, we may state that the CZTS films synthesized by sol-gel at 150^0C have smaller grains implying that they will produce a larger interface area with the n-type semiconductor in the potential PN junction. Herein, the larger crystallite size evaluated for Sample 150^0C also speaks in favour of these films, due to the expected smaller recombination electron-hole losses on the crystallite domain boundaries for those films, implying the synthesized CZTS films are expected to show better transport properties (subject to a future study). Future examination should be considered for optimization of the synthetization temperature, by testing different temperatures around the 150^0C.

5. Acknowledgement

The authors would like to acknowledge the Ministry of Higher Education of Malaysia (MOHE) through its research grant FRGS/1/2022/TK08/UKM/02/29. Appreciations are also extended to the Centre for Research and Instrumentation Management (CRIM) of Universiti Kebangsaan Malaysia (UKM), for their excellent material characterization services.

References

[1]. Ahmad, Ahmad A.; Migdadi, A. B.; Alsaad, Ahmad M.; Qattan, I. A.; Al-Bataineh, Qais M.; Telfah, Ahmad (2022): Computational and experimental characterizations of annealed Cu2ZnSnS4 thin films. In: Heliyon n. 1, 8, e08683. DOI: 10.1016/j.heliyon.2021.e08683.

[2]. Ahmed, Shafaat; Reuter, Kathleen B.; Gunawan, Oki; Guo, Lian; Romankiw, Lubomyr T.; Deligianni, Hariklia (2012): A High Efficiency Electrodeposited Cu2ZnSnS4 Solar Cell. In: Adv. Energy Mater. n. 2, 2, pp. 253–259. DOI: 10.1002/aenm.201100526.

[3]. Ahmoum, H.; Chelvanathan, P.; Su'ait, M. S.; Boughrara, M.; Li, G.; Al-Waeli, Ali H.A. et al. (2020): Impact of preheating environment on microstructural and optoelectronic properties of Cu2ZnSnS4 (CZTS) thin films deposited by spin-coating. In: Superlattices and Microstructures, 140, p. 106452. DOI: 10.1016/j.spmi.2020.106452.

[4]. Alamri, S. N. (2023): Deposition of Cu 2 ZnSnS 4 layers by a novel single flash thermal evaporator from mixture element powder. In: Journal of Taibah University for Science n. 1, 17. DOI: 10.1080/16583655.2022.2162768.

[5]. Chen, Shiyou; Gong, X. G.; Walsh, Aron; Wei, Su-Huai (2009): Crystal and electronic band structure of Cu2ZnSnX4 (X=S and Se) photovoltaic absorbers: First-principles insights. In: Appl. Phys. Lett. n. 4, 94, p. 41903. DOI: 10.1063/1.3074499.

[6]. Chen, Shiyou; Walsh, Aron; Gong, Xin-Gao; Wei, Su-Huai (2013): Classification of lattice defects in the kesterite Cu2ZnSnS4 and Cu2ZnSnSe4 earth-abundant solar cell absorbers. In: Advanced materials (Deerfield Beach, Fla.) n. 11, 25, pp. 1522–1539. DOI: 10.1002/adma.201203146.

[7]. Dwivedi, Shailendra Kumar; Tripathi, Santosh K.; Tiwari, D.C; Chauhan, Atendra S.; Dwivedi, Prabhat K.; Eswara Prasad, N. (2021): Low cost copper zinc tin sulphide (CZTS) solar cells fabricated by sulphurizing sol-gel deposited precursor using 1,2-ethanedithiol (EDT). In: Solar Energy, 224, pp. 210–217. DOI: 10.1016/j.solener.2021.04.046.

[8]. Enayati Maklavani, Shahin; Mohammadnejad, Shahram (2020): Enhancing the open-circuit voltage and efficiency of CZTS thin-film solar cells via band-offset engineering. In: Opt Quant Electron n. 2, 52. DOI: 10.1007/s11082-019-2180-6.

[9]. Fernandes, P. A.; Salomé, P.M.P.; Da Cunha, A. F. (2011): Study of polycrystalline Cu2ZnSnS4 films by Raman scattering. In: Journal of Alloys and Compounds n. 28, 509, pp. 7600–7606. DOI: 10.1016/j.jallcom.2011.04.097.

[10]. Gong, Yuancai; Zhang, Yifan; Jedlicka, Erin; Giridharagopal, Rajiv; Clark, James A.; Yan, Weibo et al. (2021): Sn4+ precursor enables 12.4% efficient kesterite solar cell from DMSO solution with open circuit voltage deficit below 0.30 V. In: Sci. China Mater. n. 1, 64, pp. 52–60. DOI: 10.1007/s40843-020-1408-x.
[11]. Guo, B. L.; Chen, Y. H.; Liu, X. J.; Liu, W. C.; Li, A. D. (2014): Optical and electrical properties study of sol-gel derived Cu 2 ZnSnS 4 thin films for solar cells. In: AIP Advances n. 9, 4, p. 97115. DOI: 10.1063/1.4895520.
[12]. He, Mingrui; Yan, Chang; Li, Jianjun; Suryawanshi, Mahesh P.; Kim, Jinhyeok; Green, Martin A.; Hao, Xiaojing (2021): Kesterite Solar Cells: Insights into Current Strategies and Challenges. In: Advanced science (Weinheim, Baden-Wurttemberg, Germany) n. 9, 8, p. 2004313. DOI: 10.1002/advs.202004313.
[13]. Ito, K. (2015): Copper zinc tin sulphide-based thin-film solar cells. Chichester: Wiley-Blackwell.
[14]. Kattan, Nessrin; Hou, Bo; Fermín, David J.; Cherns, David (2015): Crystal structure and defects visualization of Cu2ZnSnS4 nanoparticles employing transmission electron microscopy and electron diffraction. In: Applied Materials Today n. 1, 1, pp. 52–59. DOI: 10.1016/j.apmt.2015.08.004.
[15]. Kodigala, Subba Ramaiah (2014): Thin film solar cells from earth abundant materials. Growth and characterization of $Cu_2ZnSn(SSe)_4$ thin films and their solar cells. Amsterdam, Boston: Elsevier (Elsevier insights).
[16]. Kumar, Atul (2021): Efficiency enhancement of CZTS solar cells using structural engineering. In: Superlattices and Microstructures, 153, p. 106872. DOI: 10.1016/j.spmi.2021.106872.
[17]. Lai, Fang-I; Yang, Jui-Fu; Wei, Yu-Ling; Kuo, Shou-Yi (2017): High quality sustainable Cu 2 ZnSnSe 4 (CZTSe) absorber layers in highly efficient CZTSe solar cells. In: Green Chem. n. 3, 19, pp. 795–802. DOI: 10.1039/c6gc02300b.
[18]. Romanyuk, Yaroslav E.; Haass, Stefan G.; Giraldo, Sergio; Placidi, Marcel; Tiwari, Devendra; Fermin, David J. et al. (2019): Doping and alloying of kesterites. In: J. Phys. Energy n. 4, 1, p. 44004. DOI: 10.1088/2515-7655/ab23bc.
[19]. Tanaka, Kunihiko; Moritake, Noriko; Uchiki, Hisao (2007): Preparation of Cu2ZnSnS4 thin films by sulfurizing sol–gel deposited precursors. In: Solar Energy Materials and Solar Cells n. 13, 91, pp. 1199–1201. DOI: 10.1016/j.solmat.2007.04.012.
[20]. Tiong, Vincent Tiing; Bell, John; Wang, Hongxia (2014): One-step synthesis of high quality kesterite Cu2ZnSnS4 nanocrystals - a hydrothermal approach. In: Beilstein journal of nanotechnology, 5, pp. 438–446. DOI: 10.3762/bjnano.5.51.
[21]. Todorov, T.; Hillhouse, H. W.; Aazou, S.; Sekkat, Z.; Vigil-Galán, O.; Deshmukh, S. D. et al. (2020): Solution-based synthesis of kesterite thin film semiconductors. In: J. Phys. Energy n. 1, 2, p. 12003. DOI: 10.1088/2515-7655/ab3a81.